SUPPLEMENTARY TABLES & RESULTS

Table S1. Characteristics of patients included in the analysis

Parameter	No. (%)
Median age (range, years)	58 (15 - 82)
Age, 60 y or older	34 (49)
Female sex	30 (43)
Median time (months) from diagnosis to TKI	35 (1- 137)
No. Prior therapies (median, range)	4 (1 - 9)
Hemoglobin level [median level, g/dL]	[12.3]
Less than 10g/dL	4 (6)
WBC count, x 10^9/L [median count, x10^9/L]	[32.2]
Median peripheral blast % (range)	4 (0 - 9)
Median peripheral basophil % (range)	2 (0 - 8)
Median marrow blast % (range)	6 (0 - 7)
Median basophil % (range)	4 (0 - 10)
Clonal evolution present	5 (7)
Sokal risk group	
Low	26 (37)
Intermediate	24 (34)
High	20 (29)
Initial imatinib dose	
400mg/d	62 (89)
600mg/d	8 (11)
Median time (months) on imatinib (range)	35.5 (1 - 76)
Initial dasatinib dose	
<100mg/d	15 (21)
100mg/d or higher	55 (79)
Median time (months) on dasatinib (range)	20 (1 - 52)

Table S2. *BCR-ABL1* mutations detected in patients failing tyrosine kinase therapy by DNA sequencing of individual clones

Abbreviations: CP: chronic phase; AP: accelerated phase; BP: blastic phase; CHR: complete hematologic response; WT: wild-type (i.e. unmutated BCR-ABL1), na: not available

Patient	Mutation(s) (Number Clones Positive/Total Clones Examined) prior to Dasatinib	Mutations prior to Dasatinib by Direct Sequencing	Phase/Best response on Dasatinib	Mutations on Dasatinib (Number Clones Positive/Total Clones Examined)	Mutations on Dasatinib by Direct Sequencing
NO CYTOGENETIC RESPONSE ON DASATINIB					
1	H396R(3/11), WT(2/11), N297D/H396R(1/11), K247Q/H396R(1/11), T242A/K262E/H396R(1/11), V270A/M278T/H396R(1/11), M244T/H396R(1/11), del714-1021(1/11)	E355G	CP, CHR	na	na
2	L364I(4/10), L364I/A380P(1),L364I/Q346H(1),A337P(2/10), WT(2/10)	L364I	AP	na	WT
3	WT(7/10),(I242T, T394P(1/10)	WT	BP	na	na
4	WT(9/10), L301P(1/10)	WT	AP	na	V299L
5	WT(3/10),E308A(1),A287T(1), T272A(1),E352G(1),K285N(1), K247R(1),I347T/V379I/1122-1125del(1)	WT	BP	WT(4/10), L387S(1),V304D(2),N193D/V304D(2),T315I(1/10)	WT
6	WT(9/10), A344V(1/10)	WT	AP	na	WT

7	WT(8/10), R386K(1/10), V270A/S385N/G390R(1/10)	na	BP	T315I (10/10)	na
8	E255K(9/10), E255K/del858-874(1/10)	E255K	BP, not CHR		na
9	WT(8/9), Q252R(1/9)	na	AP	na	WT
10	K245E(2/10), WT(6/10), E255V(1/10), V289A(1/10)	E255V	CP, not CHR	na	E255V
11	WT(6/10), T394A(1/10), L341P(1/10), E308G(1/10), L248P(1/10)	WT	AP	na	WT
12	WT(8/10), T315I(1/10), V304D/C305Y(1/10)	WT	CP, not CHR	T315I (6/8), V304D (2/10), S410N/T315I (2/8)	T315I
13	WT(8/10), Y353H(1/10), N358S(1/10)	F486S	CP, not CHR	na	WT
14	WT(2/10), T315I(6/10), T315I/R386G(1/10), Q252L/T315I(1/10)	T315I	BP	na	na
15	WT(9/10), V304D/P310A/Y312H(1/10)	WT	CP, CHR	na	na
16	WT(3/10), M351T(5/10), L370P/M351T(1/10), W405G/M351T(1/10)	na	AP	na	T315I
17	E255V (1/20)	WT	CP, not CHR	E255V (5/10)	na
18	Y253H (3/10), M388L (3/10), L387L (3/10)	WT	CP, not CHR	Y253H (6/12), M388L (3/12), L387L (3/12)	na

19	T315I (2/10), F359V (6/10), G250E (1/10), M244V (1/10)	WT	CP, not CHR	T315I(3/10), F359V(2/10)	na
20	M244V (10/10)	WT	CP, not CHR	M244V (10/10)	na
21	F359I (9/9)	WT	CP, not CHR	F359I (6/10)	na
22	H396R (4/12), M351T (4/12), Q252R (1/12)	WT	CP, not CHR	H396R(5/10), M351T(5/10)	na
23	K271R(2/10), WT(4/10), F317L(1/10), E282G(1/10), L298V/G303E/V304D/N336D/F317L(1/10), L298V/L387S(1/10)	F317L	CP, not CHR	V304D(6/10), F317L(3/10), V304D/F317L(1/10)	na
24	WT(6/8), K400N(1/8), E292G/A399T(1/8)	na	BP, CHR	na	na
25	WT(5/10), A366T(1/10), D233G(1/10), T389A(1/10), T394I(1/10), T267A(1/10)	F317L	BP	F317L(10/10)	na
26	WT(8/10), V304D(1/10), D276N/V304D(1/10)	WT	BP	na	na
27	WT(9/10), A380T(1)	na	BP	na	na
28	WT(5/11), F311L/T382A(1/11), R362T(1/11), Y273C/N349D(1/11), Y257C/K262M(1/11), Y393H(1/11), D325G/I403T(1/11)	WT	CP, not CHR	na	WT
29	F317L(5/8), V304D(3/8)	F317L	CP, not CHR	V299L(4/5), WT(1/5)	F317L

30	G250E(2/10), G250E/E409K(1/10), G250E/L364I/A365D/G372W/E373D(1/10), E255V/F382Y(1/10), E255V(5/10)	na	CP, not CHR	T315I(5/5)	na
	MINOR CYTOGENETIC RESPONSE ON DASATINIB				
31	M351T(4/5), V304D/M351T(1)	na	CP, not CHR	na	F317L
32	WT(6/6)	na	na	na	na
33	WT(5/6)	na	CP, not CHR	na	F359V, F311L
34	V304D(4/6), V338E(1/10), E316G(1/6)	WT	CP, not CHR	na	WT
35	E255K(7/10), E255K/V304D(3/10)	na	BP, not CHR	na	na
36	WT(6/8), V304D(2/8)	G250E	AP, not CHR	WT(5/10), G250E(3/8)	na
37	WT(8/10), Y264S(1/10), del750-820;194-196	na	BP	WT (4/9), L355Q/I360N(1/9), A377T (1/9), V299L/V338M(1/9), V299L(1/9), E250G/V299L/T272I(1/9)	na
38	Y253H(8/10), R307G/Y253H(2/10)	M244V, M351T	BP	Y253H/F317I (3/10), T315I/Y253H (6/10), V304D/Y253H/T315I (1/10)	na
39	WT(7/8), E291V(1/8)	E292V	BP, CHR	na	na
40	E255K (12/12)	WT		E255K (10/10)	na

41	E355G (8/10), E355G/Q252R (1/10)	WT		E355G(8/10), Q252R(1/10)	na
PARTIAL CYTOGENETIC RESPONSE ON DASATINIB					
42	WT(8/10), L302P(2/10)	WT	CP, CHR	na	na
43	E355G(8/11),E238G/E355G(1/11),V338A/E355G(1/11),N368D/E355G(1/11)	E355G (3/04)	BP	E355G(2/8), WT(3/8), M351T/E355G(1/8), N368D/E355G(1/8), I360T(1/8)	E355G
44	WT(8/10),L411Q(1/10),F311S(1)	WT	BP	na	WT
45	WT(8/8)	Y253H	AP, not CHR	na	WT
46	WT(10/10)	WT	BP, not CHR	na	WT
47	M351T (4/10), F359C (2/10)	WT	CP, CHR	na	na
48	G250E (9/10), G250E/F317L (1/10)	WT	CP, CHR	G250E(10/10)	na
COMPLETE CYTOGENETIC RESPONSE ON DASATINIB					
49	WT(6/12), H295R(1/12), R328G(1/12), T267A(1/12), L387S(1/12), A344V/N374Y(1/12), M351V(1/12)	WT	CP, not CHR	na	F486S, V299L
50	G250E(9/12),L395S/G250E(1), M337T/G250E(1)	na	CP, not CHR	na	G250E
51	WT(8/12), M244L(1/12), V304D/N358D/F359S(1/12), E282A(1/12), R386G(1/12)	WT	CP, CHR	na	na
52	WT(8/8)	WT	AP, CyR		WT

53	WT(7/10), D363H/A399P(1/10), N221K/Y232H/M343I/E355Q(1/10), I314V(1/10)	WT	CP, not CHR	na	WT
54	M351T(9/10), N231/M351T(1/10)	M351T	CP, not CHR	na	na
55	L387M(7/10), L248V/L387M(1/10), D421G/L387M(1/10), WT(1/10)	L387M	CP, CHR	L387M	na
56	WT (10/10)	WT	CCyR	WT(10/10)	na
57	M351T (11/11)	WT	CCyR	M351T(10/10)	na
58	G250E (10/10)	WT	CCyR	G250E(10/10)	na
59	S417Y (10/10)	WT	CCyR	S417Y(10/10)	na
60	M244V (12/12)	WT	CCyR	M244V (10/10)	na
61	M351T (8/9), M351S (1/9)	WT	CCyR	M351T(6/10), M244V(4/10)	na
62	WT (11/11)	WT	CCyR	WT	na
63	Y253H (11/11)	WT	CCyR	Y253H(10/10)	na
64	WT (12/12)	WT	CCyR	WT	na
65	WT (11/11)	WT	CCyR	WT	na
66	G250E(6/8),Y234R/G250E(1/8), V371A/G250E(1/8)	G250E	AP	na	na
67	WT(8/10), N193D(2/10)	na	BP, no CHR		
68	WT(8/12), E283S/K285T/E286D(1/12), E352K(1/12), H246Y(1/12), V260L/E258Y(1/12)	WT	CP, PCyR	na	na
	NOT EVALUABLE FOR CYTOGENETIC RESPONSE				
69	WT(7/8), M343I(1/8)	WT	BP, not CHR	na	na

70	WT(5/10), V304D(5/10)	WT	BP, not CHR	na	na

SUPPLEMENTARY RESULTS

Study group

We evaluated 70 patients with CML-CP who developed resistance to imatinib and subsequently were enrolled in phase I and II studies of dasatinib (Table S1). The median age was 58 years (range, 15-82) and the median number of prior therapies was 4 (range, 1-9). The median time from diagnosis to imatinib therapy was 35 months (range, 1-137). The initial imatinib dose was 400 mg/day in 60 patients, 600 mg/day in 8, and 800 mg/day in 2 patients.

Mutational status after imatinib failure

Upon imatinib failure, *BCR-ABL1* kinase domain mutations were detected in 61 (87%) of 70 patients by DNA expansion of specific clones, including 38 (54%) with mutations detected in ≥20% of sequenced clones. In contrast, *BCR-ABL1* mutations were detected in only 18 (47%) of 38 patients when direct sequencing was employed in available samples. Overall, 125 mutations at 113 amino acid positions were detected by DNA expansion of specific clones, including 78 which had not been previously reported (Table S2). Mutations known to confer resistance to >1μM imatinib (M244V, G250E, Q252H, Y253H, E255K/V, F359V, H396R, and T315I) were detected in 30 (43%) of 70 patients by DNA expansion of specific clones after imatinib failure, but only in 5 (13%) of 38 by direct sequencing. Of note, 2 or more mutations within the same clone (*polymutants*) were detected in 29 (41%) of 70 patients, with individual clones expressing 2 (n=38), 3 (n=11), 4 (n=1), or even 5 (n=2) single point mutations (Figure S1A). By contrast, only 1 patient was found to carry 2 different mutations (M244V and M351T) when using direct sequencing techniques. These data indicate that the use of molecular techniques with higher sensitivity relative to conventional direct sequencing of *BCR-ABL1* can detect mutations in most patients acquiring resistance to imatinib. Furthermore, at variance with previously reported data,[1] the emergence of polymutants not only occurs after failure of a second TKI (e.g. dasatinib) but it is rather prevalent following failure of frontline imatinib therapy.

Mutational status during dasatinib therapy

Dasatinib therapy was administered for a median of 20 months (range, 2-52). Sixty-eight (97%) of 70 patients were assessable for response. Overall, the CHR rate was 66% while the MCyR was 34%, including a CCyR rate of 25%. Eighteen (26%)

patients only achieved CHR and 18 (26%) only had partial hematologic response. Three (4%) patients did not achieve any response with dasatinib therapy. DNA expansion of specific clones was performed in 32 (47%) patients during dasatinib therapy and revealed 20 additional mutations not present at dasatinib start, which involved 19 distinct amino acid positions (Table S2). Five of the additional mutations have never been previously reported and all were involved in polymutant clones. Dasatinib-resistant mutations (L248V/R, Q252H, E255K, V299L, T315I/A, and F317L/C/I/S/V) were detected in 10 (31%) of 32 patients by DNA expansion of specific clones (including 5 who carried T315I). Of the latter 32 patients, 16 (50%) were simultaneously evaluated by direct sequencing, which only detected dasatinib-resistant mutations in 3 (19%) patients. All those 16 patients died after progression to blast phase**.**

Mechanisms of resistance of BCR-ABL1 V299L, T315I, and F317L: proof-of-concept of the in silico methodology

Table S3 lists the computational results obtained for unmutated and single point BCR-ABL1 mutants in complex with imatinib or dasatinib.

For imatinib, all single missense BCR-ABL1 mutations detected in clinical specimens can be classified into three major classes (Table S3): a) *sensitive*, for which the IC_{50} fold change (FC) with respect to the unmutated kinase is <25 (V299L, V304); b) *partially sensitive*, for which the IC_{50} fold change with respect to unmutated BCR-ABL1 is >25 and <50 (Q252H, F317L, F359V, and H396R); and c) resistant, for which the fold change in IC_{50} relative to the unmutated kinase is >50 (G250E, L248R, E255K, Y253H, and T315I). For dasatinib, the mutant kinases T315I, V299L, L248R and F317L are extremely resistant, E255K and Q252H exhibit partial sensitivity, while all remaining mutants retain considerable affinity for this TKI.

According to both clinical and computational data, the V299L mutant isoform of BCR-ABL1 is highly resistant to dasatinib whereas no effect on imatinib binding has been observed so far. A detailed energetic analysis of the unmutated BCR-ABL1 binding site in complex with imatinib (Table S4) revealed that the residues lining the inhibitor docking pocket afford an overall stabilizing contribution of ΔG_{bind}^{bs} = –8.02 kcal/mol, 4 residues yielding a ΔG_{bind}^{bs} value larger than 1 kcal/mol (highlighted in bold in Table S4). Importantly, this analysis also showed that residue 299 does not contribute to imatinib binding. Consequently, substitution of valine by leucine at this

position does not cause a substantial modification of the overall binding site energy ($\sum \Delta G_{bind}^{bs}$ = -7.68 kcal/mole), which justifies the sensitivity of this mutant to imatinib.

Table S3. Predicted free energy of binding (ΔG_{bind}), IC_{50} and fold change (FC) values for BCR-ABL1 single point mutants and imatinib or dasatinib

	BCR-ABL1	$IC_{50[exp]}$(nM)*	ΔG_{bind} (kcal/mol)	IC_{50} (nM)§	FC
imatinib	Unmutated	25 – 527[a-e]	-10.47 ± 0.03	21	-
	T315I	>3000[a-e]	-6.83 ± 0.03	21000	1000
	Y253H	4000 – 18000[b,c,e]	-7.45 ± 0.02	3400	162
	E255K	>3000[b-e]	-7.56 ± 0.02	2877	137
	L248R	>7000[b,e]	-7.82 ± 0.03	1900	90
	G250E	1350 – 4800[b-e]	-8.14 ± 0.01	1090	52
	H396R	1750 – 2058[c-e]	-8.20 ± 0.02	987	47
	F359V	1509 – 1825[c-e]	-8.25 ± 0.01	903	43
	F317L	1050 – 1583[b-e]	-8.31 ± 0.02	819	39
	Q252H	734 – 2900[b-e]	-8.32 ± 0.01	798	38
	M244V	454 – 3100[b,c,e]	-8.50 ± 0.02	590	28
	V299L	540 – 814[c-e]	-9.58 ± 0.03	105	5
	V304D	-	-9.87 ± 0.02	59	2.8
dasatinib	Unmutated	0.6 – 1.8[c-g]	-12.39 ± 0.01	0.8	-
	T315I	>137[c-e,g]	-6.44 ± 0.02	19000	23750
	V299L	15.8 – 18[c-e,g]	-8.21 ± 0.01	960	1200
	L248R	16 – 23[e,g]	-8.67 ± 0.01	317	396
	F317L	7.4 – 18[c-e,g]	-9.23 ± 0.03	170	213
	E255K	5.6 – 13[c-e,g]	-10.77 ± 0.02	12.8	16
	Q252H	3.4 – 5.6[c-e]	-10.85 ± 0.01	11.2	14
	Y253H	1.3 – 10[c,e,g]	-11.08 ± 0.02	7.6	9.5
	H396R	1.3 – 3.0[c-e]	-11.98 ± 0.04	1.7	2.1
	F359V	2.2 – 2.7[c-e]	-12.00 ± 0.02	1.6	2
	M244V	1.3 – 3.6[c,e]	-12.22 ± 0.02	1.4	1.8
	V304D	-	-12.27 ± 0.01	1	1.3
	G250E	1.8 – 8.1[c-e]	-12.31 ± 0.02	0.96	1.2
ponatinib	Unmutated	0.5 - 2.1[e,h,i]	-12.67 ± 0.02	0.52	-
	E255K	14 - 17.6[e,h]	-10.99 ± 0.01	8.8	17
	T315I	6.3 - 11[e,h,i]	-11.10 ± 0.01	7.4	14
	G250E	4.1 - 12.5[e,h]	-11.14 ± 0.01	6.9	13
	H396R	12.5[e]	-12.13 ± 0.02	1.3	2.5
	V299L	1.2[e]	-12.13 ± 0.02	1.3	2.5
	F317L	1.1 - 1.5[e,h]	-10.81 ± 0.03	1.2	2.3
	M244V	2.2 - 6.7[e,h]	-12.23 ± 0.01	1.1	2.1
	F359V	9.2 – 10[e,h]	-12.41 ± 0.01	0.81	1.6
	Q252H	2.2 - 12.9[a,c]	-12.42 ± 0.02	0.79	1.5
	V304D	-	-12.48 ± 0.02	0.72	1.4
	Y253H	5.4 - 6.2[e,h]	-12.64 ± 0.03	0.55	1.1

[§]ΔG_{bind} and the concentration of ligand that inhibits the kinase activity by 50% (i.e., IC_{50}) are related by the following fundamental equation: ΔG_{bind} = -RTln $1/IC_{50}$. Thus, once ΔG_{bind} for a given kinase/inhibitor couple is estimated, the relative IC_{50} value is also known by virtue of this relationship. *Data from: [a]Corbin et al. *J Biol Chem*. 2002, 277:32214-19. [b]Walz et al. *Crit Rev Oncol Hematol.* 2006, 57:145-64. [c]O'Hare et al. Blood 2007, 110:2242-2249. [d]Redaelli et al. *J Clin Oncol.* 2009 27:469-71.[e]Redaelli et al. *Am J Hematol.* 2012, 87:E125-8. [f]Puttini et al. *Cancer Res.* 2006, 66:11314-11322. [g]Burgess et al. *PNAS* 2005, 102:3395-3400.[h]O'Hare et al. *Cancer Cell* 2009, 16:401-412. [i]Huang et al. *J Med Chem.* 2010, 53:4701-4719.

Table S4. **Per-residue free-energy decomposition for WT and V299L BCR-ABL1 in complex with imatinib**

	WT	V299L
	ΔG_{bind}^{bs} (kcal/mol)	$\Delta G_{\mathrm{bind}}^{\mathrm{bs}}$ (kcal/mol)
Y253	-0.81	-0.73
E286	-0.81	-0.60
V299/L	0.00	0.00
T315/I	**-1.03**	-0.95
F317	**-1.62**	**-1.54**
M318	**-1.02**	-0.89
I360	-**1.00**	**-1.03**
H361	-0.68	-0.77
D381	-0.31	-0.56
F382	-0.74	-0.61
$\sum \Delta G_{bind}^{bs}$ (kcal/mol)	**-8.02**	**-7.68**

The same analysis performed on the analogous BCR-ABL1 complexes with dasatinib (Table S5) not only confirms that the unmutated BCR-ABL1 binding site residues are more efficient in stabilizing the drug within the kinase pocket with respect to imatinib ($\sum \Delta G_{\mathrm{bind}}^{\mathrm{bs}}$ = -9.92 kcal/mol), but perhaps more importantly, that dasatinib resistance associated with the V299L mutation cannot be totally ascribed to a disruption of the binding site conformation, as the overall stabilization energy of the binding site is only slightly decreased with respect to the unmutated kinase ($\sum \Delta G_{bind}^{bs}$ = -9.07 kcal/mol). Therefore, other molecular mechanisms are likely contributing to the poor affinity of V299L for dasatinib.

Mutations in the P-loop and A-loop of the BCR-ABL1 kinase destabilize its inactive conformation, thus favoring an active state that impairs the binding of TKIs like imatinib that target its inactive conformation.[2-7] Other mutations induce TKI resistance directly by causing steric hindrance within the ATP binding cleft.[2-7] Several of these mechanisms can exist simultaneously. X-ray spectroscopy of tyrosine kinases has revealed that shifting from a closed (inactive) to an open (active) conformation involves changes in position and orientation of multiple residues at the activation loop and at the catalytic C-helix.[2-7] A network of highly conserved

hydrophobic or amino-aromatic interactions – commonly termed the *hydrophobic spine*– involving residues M290, L301, H361, and F382 is stabilized during BCR-ABL1 kinase activation.[4,8] Thus, we extended our analysis to unveil interactions between some of the amino acid substitutions encountered in our patient cohort and the spine residues that might lead to stabilization of the spine and ultimately TKI resistance. To the purpose, we applied a *per-residue* decomposition analysis to the residues involved in the spine hydrophobic interactions in the unmutated BCR-ABL1 protein in complex with imatinib and dasatinib (Table S6).

Table S5. Per-residue free-energy decomposition for WT and V299L BCR-ABL1 in complex with dasatinib

	WT	V299L
	ΔG_{bind}^{bs} (kcal/mol)	ΔG_{bind}^{bs} (kcal/mol)
L248	-0.95	-0.99
M290	**-1.18**	-0.69
V299/L	**-1.54**	**-1.12**
I313	**-1.36**	**-1.53**
T315	**-1.15**	-0.88
E316	-0.48	-0.11
F317/L	**-1.71**	**-1.94**
M318	-0.08	-0.38
T319	**-1.47**	**-1.43**
$\sum \Delta G_{bind}^{bs}$ (kcal/mol)	**-9.92**	**-9.07**

Table S6. **Hydrophobic spine per-residue free-energy decomposition for WT BCR-ABL1 in complex with imatinib or dasatinib. All values are in kcal/mol. Data standard deviations are in the range ±0.01 ÷ ±0.05**

imatinib	V299	L301	T315	F317	H361	F382
M290	**-0.35**	**-1.6**	**-0.25**	-0.01	-0.01	-0.01
V299	*	**-0.35**	**-0.68**	**-0.11**	-0.01	-0.05
L301	*	*	**-0.75**	-0.03	0.00	0.00
T315	*	*	*	**-0.40**	0.00	-0.02
F317	*	*	*	*	0.00	-0.01
H361	*	*	*	*	*	**-0.13**
ΔG_{bind}^{spine}						**-4.8**
dasatinib	V299	L301	T315	F317	H361	F382
M290	**-0.81**	**-1.6**	-0.06	-0.01	-0.02	**-0.40**
V299	*	**-0.56**	**-0.21**	-0.08	-0.01	**-0.29**
L301	*	*	**-0.71**	-0.04	0.00	-0.03
T315	*	*	*	**-0.55**	0.00	-0.05
F317	*	*	*	*	0.00	0.00
H361	*	*	*	*	*	**-1.7**

ΔG_{bind}^{spine}	**-7.1**

For imatinib, which binds to the inactive WT BCR-ABL1 conformation, the stabilization energy of the hydrophobic spine (ΔG_{bind}^{spine} = -4.8 kcal/mol) is substantially lower than in the case of the WT active conformation favorable to dasatinib binding (ΔG_{bind}^{spine} = -7.1 kcal/mol), as expected.

Interestingly, however, in the presence of the BCR-ABL1 V299L mutation, the hydrophobic spine is less straightened when the protein is bound to dasatinib, as shown in Table S7. This effect is mainly ascribable to the altered conformation of the leucine residue that loses interaction with M290 for approximately 0.5 kcal/mol with respect to the WT case (Figure 2B and Tables S6 & S7).

Table S7. **Hydrophobic spine per-residue free-energy decomposition for V299L BCR-ABL1 in complex with imatinib and dasatinib. All values are in kcal/mol. Data standard deviations are in the range ±0.01 ÷ ±0.05**

imatinib	L299	L301	T315	F317	H361	F382
M290	-**0.29**	-**1.7**	-**0.31**	-0.01	0.00	0.00
L299	*	-**0.30**	-**0.70**	-0.06	-0.01	-0.03
L301	*	*	-**0.81**	-0.02	0.00	0.00
T315	*	*	*	-**0.49**	0.00	-0.01
F317	*	*	*	*	0.00	-0.01
H361	*	*	*	*	*	-**0.24**
ΔG_{bind}^{spine}						**-5.0**
dasatinib	L299	L301	T315	F317	H361	F382
M290	-**0.30**	-**1.3**	-**0.32**	-0.01	-0.02	-0.01
L299	*	-**0.29**	-**0.80**	-0.03	-0.01	-0.01
L301	*	*	-**0.72**	-0.01	0.00	-0.02
T315	*	*	*	-**0.53**	0.00	-0.04
F317	*	*	*	*	0.00	0.00
H361	*	*	*	*	*	-**0.63**
ΔG_{bind}^{spine}						**-5.1**

Again in the case of V299L BCR-ABL1 mutant in complex with dasatinib, a weaker interaction with H361 causes a specific repositioning of F382 in the DFG motif towards an intermediate conformation between the "in" and "out" states. Accordingly, a weaker hydrophobic interaction with the F382 residue in the intermediate conformation may act as a trigger to facilitate the transition from the active DFG-in to the inactive DFG-out state. The proposed structural mechanism thus might initiate the disruption of the spine and cause imbalance in the dynamic

equilibrium between the active (to which dasatinib binds) and inactive conformation states regulating the kinase, ultimately leading to decreased drug affinity[9]. The critical role of residue F382 in the spine stabilization is highlighted by the considerably more favorable interaction energies of this residue with M290, V299, and, especially, H361 in the case of dasatinib. Also, the significant interaction of M290 and L301 seems to be preserved in both BCR-ABL1 kinase conformations, in agreement with crystallographic data.

T315 and F317 are two extremely deleterious mutations leading to enhanced drug resistance to both imatinib and dasatinib (Table S3). The application of the same per-residue analysis to the gatekeeper T315I BCR-ABL1 mutant isoform in complex with imatinib clearly shows that the presence of the bulkier, hydrophobic isoleucine residue causes a destabilization of the overall asset of the hydrophobic spine and the subsequent adoption of an intermediate conformation between an active and inactive kinase state (Table S8). On the contrary, a missense mutation in a drug contact point such as F317L exerts a direct, somewhat more classical effect on drug affinity by altering the tailored fitting of the binding site without any effect on the spine stabilization/destabilization (last column panel in Figure 2C & upper part of Table S8).

Table S8. **Hydrophobic spine per-residue free-energy decomposition for T315I BCR-ABL1 in complex with imatinib and F317L BCR-ABL1 in complex dasatinib, respectively. All values are in kcal/mol. Data standard deviations are in the range ±0.01 ÷ ±0.05**

imatinib	V299	L301	I315	F317	H361	F382
M290	**-0.75**	**-1.5**	**-0.30**	0.00	-0.01	**-0.30**
V299	*	**-0.60**	**-0.83**	-0.05	0.00	-0.02
L301	*	*	**-0.70**	-0.01	0.00	-0.02
I315	*	*	*	**-0.43**	-0.01	0.00
F317	*	*	*	*	0.00	-0.01
H361	*	*	*	*	*	**-1.2**
ΔG_{bind}^{spine}						**-6.8**
dasatinib	V299	L301	T315	L317	H361	F382
M290	**-0.78**	**-1.6**	**-0.18**	-0.10	-0.01	**-0.43**
V299	*	**-0.50**	**-0.28**	-0.08	-0.01	**-0.20**
L301	*	*	**-0.69**	-0.03	0.00	-0.03
T315	*	*	*	**-0.33**	0.00	-0.09
L317	*	*	*	*	-0.01	0.00
H361	*	*	*	*	*	**-1.6**
ΔG_{bind}^{spine}						**-7.0**

An analogous situation is observed in the case of the drug-contact F317L mutant in complex with dasatinib (lower part of Table S8): as shown, several contacts with critical residues such as M290 are lost, leading to rearrangement of the binding site which, in turn, results in a substantially lower affinity of the kinase for the drug. Overall, in the case of the T315I mutant in complex with imatinib, the hydrophobic spine results to be remarkably stabilized (= -6.8 kcal/mol) with respect to the unmutated BCR-ABL1 kinase (ΔG_{bind}^{spine} = -4.8 kcal/mol). Conversely, in the case of dasatinib, the direct replacement of phenylalanine by a leucine residue at position 317 has virtually no effect on the spine stabilization/destabilization, as the estimated ΔG_{bind}^{spine} values for the unmutated and F317L isoforms are almost identical (-7.1 kcal/mol and -7.0 kcal/mol, respectively).

Table S9. Per-residue free-energy decomposition for unmutated, T315I and T315I/V299L BCR-ABL1 in complex with imatinib

	WT	T315I	T315I/V299L
	ΔG_{bind}^{bs} (kcal/mol)	ΔG_{bind}^{bs} (kcal/mol)	ΔG_{bind}^{bs} (kcal/mol)
Y253	-0.81	-0.20	-0.14
E286	-0.81	-0.65	-0.38
V299/L	0.00	-0.01	0.10
T315/I	**-1.03**	**-1.70**	**-1.78**
F317	**-1.62**	**-1.22**	-0.92
M318	**-1.02**	-0.68	-0.58
I360	**-1.00**	-0.69	-0.51
H361	-0.68	-0.48	-0.41
D381	-0.31	-0.26	-0.34
F382	-0.74	-0.82	-0.68
$\sum \Delta G_{bind}^{bs}$ (kcal/mol)	**-8.02**	**-6.71**	**-5.64**

Table S10. Per-residue free-energy decomposition for WT, F317L, and F317L/V299L BCR-ABL1 in complex with dasatinib

	WT	F317L	F317L/V299L
	ΔG_{bind}^{bs} (kcal/mol)	ΔG_{bind}^{bs} (kcal/mol)	ΔG_{bind}^{bs} (kcal/mol)
L248	-0.95	-0.76	-0.73
M290	**-1.18**	-0.54	-0.61
V299/L	**-1.54**	**-1.28**	**-1.04**
I313	**-1.36**	**-1.87**	**-1.53**
T315	**-1.15**	-0.65	-0.52
E316	-0.48	-0.40	-0.71
F317/L	**-1.71**	-0.34	-0.34
M318	-0.08	-0.40	-0.38
T319	**-1.47**	**-1.63**	**-1.55**
$\sum \Delta G_{bind}^{bs}$ (kcal/mol)	**-9.92**	**-7.87**	**-7.41**

Table S11. Per-residue free-energy decomposition for WT, V299L, and F317L BCR-ABL1 in complex with ponatinib

	WT	V299L	F317L
	ΔG_{bind}^{bs} (kcal/mol)	ΔG_{bind}^{bs} (kcal/mol)	ΔG_{bind}^{bs} (kcal/mol)
L248	**-1.01**	-0.99	-0.98
Y253	**-1.74**	**-1.68**	**-1.64**
E286	**-1.36**	**-1.33**	**-1.31**
I293	-0.56	-0.55	-0.56
V299/L	-0.38	-0.29	-0.25
T315	-0.72	-0.81	-0.65
F317/L	**-1.70**	**-1.66**	**-1.55**
M318	**-1.81**	**-1.76**	**-1.63**
I360	-0.31	-0.33	-0.31
H361	**-1.56**	**-1.52**	**-1.48**
D381	-0.52	-0.50	-0.51
3	**-11.67**	**-11.42**	**-10.87**

Supplemental computational details

All parallel molecular dynamics (MD) simulations and the relevant analyses were performed using both Amber 9 and Amber 11 suites of programs[10-11] running on 256 processors on the IBM SP6 at the CINECA supercomputer center (Bologna, Italy). Molecular graphic images were produced using the UCSF Chimera package from the Resource for Biocomputing, Visualization, and Informatics at the University of California, San Francisco (supported by NIH P41 RR-01081)[12].

In the generation of all BCR-ABL1/inhibitor molecular complexes studied in this work, the following available structures of BCR-ABL1 co-crystallized with the different tyrosine kinase inhibitors (TKIs) were employed as starting models: 1IEP.pdb (wild-type BCR-ABL1 in complex with imatinib)[13], 2GQG.pdb (wild-type BCR-ABL1 in complex with dasatinib)[14], 2V7A.pdb (T315I mutant BCR-ABL1 in complex with danusertib)[15], 3OXZ.pdb (wild-type BCR-ABL1 in complex with ponatinib)[16], and 3IK3.pdb (T315I mutant BCR-ABL1 in complex with ponatinib)[17].

The original crystal structures of the kinase/TKI complexes were inspected for integrity, and in the case of the 3OXZ.pdb file, the small, missing loops (274-279 (KEDTME), 386-392 (RLMTGDT), and 395-397 (AHA)) were built and optimized using the *Loop Refinement* modulus of the MODELER suite implemented in Discovery Studio (v.2.5, Accelrys, San Diego, CA, USA). The Amber *ff03* force field[18] was used to parametrize the kinase structures. The atomic partial charges for all TKIs were obtained using the RESP procedure[19], and the electrostatic potentials were produced by single-point quantum mechanical calculations at the Hartree-Fock level with a 6-

31G* basis set, using the Merz-Singh-Kollman van der Waals parameters[20-21]. Eventual missing force field parameters for the inhibitor molecules were generated using the Antichamber tool[22] of Amber 9/11 and the general AMBER force field (GAFF) for rational drug design.[23]

The structures of each mutant and double mutant BCR-ABL1 in complex with the different TKIs that were obtained exploited a well-validated procedure reported in details in our previous work.[24] Figure S7 shows a comparison between the optimized, available crystal T315I mutant BCR-ABL1 in complex with ponatinib and the optimized structure of the same complex as obtained by applying our *in silico* mutagenesis procedure, as an example. As can be seen, the agreement between the two structures is excellent.

Each BCR-ABL1/TKI complex was then allowed to relax in a 90Å × 90Å × 90Å box of TIP3P water molecules[25]. The resulting system was minimized with a gradual decrease in the position restraints of the protein atoms. Finally, to achieve electroneutrality, a suitable number of neutralizing ions were added; further, the solution ionic strength was adjusted to the physiological value of 0.15 M by adding the required amounts of Na^+ and Cl^- ions. After energy minimization of the added ions for 1500 steps, keeping the protein, the ligand, and the pre-existing waters rigid, followed by an MD equilibration of the entire water/ion box with fixed solute for 2 ns, further unfavorable interactions within the structures were relieved by progressively smaller positional restraints on the solute (from 25 to 0 kcal/(mol $Å^2$) for a total of 5 ns. Each hydrated complex system was gradually heated to 310 K in three intervals, allowing a 2 ns interval per each 100 K, and then equilibrated for 5 ns at 310 K, followed by 50 ns of data collection runs, necessary for the estimation of the free energy of binding (*vide infra*).

The MD simulations were performed at constant T = 310 K using the Berendsen et al. algorithm[26] with an integration time step of 2 fs, and the applications of the Shake algorithm[27] to constrain all bonds to their equilibrium values, thus removing high frequency vibrations. Long-range nonbonded van der Waals interactions were truncated by using a dual cutoff of 9 and 13 Å, respectively, where energies and forces due to interactions between 9 and 13 Å were updated every 20-time steps. The particle mesh Ewald method[28] was used to treat the long-range electrostatics. For the calculation of the binding free energy between BCR-ABL1 and each inhibitor in water, a total of 50000 snapshots were saved during the MD data collection period described above.

The binding free energy ΔG_{bind} of each BCR-ABL1/TKI complex in water was calculated according to the procedure termed Molecular Mechanic/Poisson-Boltzmann Surface Area (MM/PBSA), and originally proposed by Srinivasan et al[29]. The theoretical background of this methodology is described in details in the original papers by Peter Kollman and collaborators[30], and has been successfully employed by our group in related studies.[24] Briefly, an MD simulation (typically in explicit solvent) was first carried out which yields a representative ensemble of structures. The average total free energy of binding between each drug and the protein receptor was then calculated as:

$$\Delta G_{bind} = \Delta E_{MM} + \Delta G_{solv} - T\Delta S \quad (1)$$

where ΔG_{bind} is the binding free energy in water, ΔE_{MM} is the interaction energy between the inhibitor and the kinase, ΔG_{solv} is the solvation free energy, and $-T\Delta S$ is the conformational entropy contribution to the binding. ΔE_{MM} is calculated from the molecular mechanics (MM) interaction energies, according to:

$$\Delta E_{MM} = \Delta E_{ele} + \Delta E_{vdw} \quad (2)$$

where ΔE_{ele} and ΔE_{vdw} are electrostatic and van der Waals interaction energies between the TKI and the kinase, which are calculated using the MM/PBSA module in the Amber 9/11 software suites.

The solvation energy, ΔG_{solv}, is divided into two parts, the electrostatic contributions, $\Delta G_{solv,pol}$, and all other contributions, $\Delta G_{solv,nonpol}$:

$$\Delta G_{solv} = \Delta G_{solv,pol} + \Delta G_{solv,nonpol} \quad (3)$$

The electrostatic contribution to the solvation free energy, $\Delta G_{solv,pol}$, is calculated using the DelPhi software package[31], which solves the Poisson-Boltzmann equations numerically and calculates the electrostatic energy according to the electrostatic potential. Interior and exterior dielectric constant values e were set equal to 1 and 80, respectively. A grid spacing of 2/Å, extending 20% beyond the dimensions of the solute, was employed. The non-polar component $\Delta G_{solv,nonpol}$ was obtained using the following relationship[32]: $\Delta G_{solv,nonpol} = \gamma \times SA + \beta$, in which γ = 0.00542 kcal/(mol Å^2), β = 0.92 kcal/mol, and the surface area SA was estimated by means of the MSMS software[33].

The quasi-harmonic analysis[34] was then employed directly to obtain the last term in equation (1) i.e., the change in solute entropy upon association $-T\Delta S$, from the Cartesian-coordinate covariance matrix accumulated during the corresponding molecular dynamics trajectory. To minimize the effects due to different conformations adopted by individual snapshots we averaged the estimation of entropy over 5000 snapshots. Finally, the IC_{50} values were calculated from the corresponding binding free energies using the following relationship[35]:

$$\Delta G_{bind} = RT \ln K_{diss} \cong RT \ln IC_{50} \quad (4)$$

The contribution of each kinase residue belonging to the so-called "hydrophobic spine" to the stabilization/destabilization of the active/inactive protein conformation and its eventual relation to drug resistance was investigated by means of component analysis.[36] Accordingly, a per residue binding free energy decomposition was performed exploiting the MD trajectory of each given inhibitor/kinase complex. This analysis was carried out using the MM/GBSA approach,[37] and was based on the same snapshots used in the binding free energy calculation.

All BCR-ABL1/inhibitor complex structures remained stable for all 50 ns of the corresponding MD trajectories, as indicated by the small fluctuations of the root-mean-square deviation (RMSD) of the simulated position of the protein backbone atoms with respect to those of the initial structure and the corresponding temperature and total potential energy of the system as shown in Figure S8 for the wild type BCR-ABL1/imatinib complex as an example.

SUPPLEMENTARY REFERENCES

1. Shah NP, Skaggs BJ, Branford S, et al. Sequential ABL kinase inhibitor therapy selects for compound drug-resistant BCR-ABL mutations with altered oncogenic potency. J Clin Invest 2007;117:2562-9.

2. Shah NP, Nicoll JM, Nagar B, et al. Multiple BCR-ABL kinase domain mutations confer polyclonal resistance to the tyrosine kinase inhibitor imatinib (STI571) in chronic phase and blast crisis chronic myeloid leukemia. Cancer Cell 2002;2:117-25.

3. Gorre ME, Mohammed M, Ellwood K, et al. Clinical resistance to STI-571 cancer therapy caused by BCR-ABL gene mutation or amplification. Science 2001;293:876-80.

4. Azam M, Seeliger MA, Gray NS, Kuriyan J, Daley GQ. Activation of tyrosine kinases by mutation of the gatekeeper threonine. Nat Struct Mol Biol 2008;15:1109-18.

5. Roumiantsev S, Shah NP, Gorre ME, et al. Clinical resistance to the kinase inhibitor STI-571 in chronic myeloid leukemia by mutation of Tyr-253 in the Abl kinase domain P-loop. Proc Natl Acad Sci U S A 2002;99:10700-5.

6. DiNitto JP, Wu JC. Molecular mechanisms of drug resistance in tyrosine kinases cAbl and cKit. Crit Rev Biochem Mol Biol;46:295-309.

7. Young MA, Shah NP, Chao LH, et al. Structure of the kinase domain of an imatinib-resistant Abl mutant in complex with the Aurora kinase inhibitor VX-680. Cancer Res 2006;66:1007-14.

8. Kornev AP, Haste NM, Taylor SS, Eyck LF. Surface comparison of active and inactive protein kinases identifies a conserved activation mechanism. Proc Natl Acad Sci U S A 2006;103:17783-8.

9. Laurini E, Posocco P, Fermeglia M, Gibbons DL, Quintás-Cardama A, Pricl S. Through the open door: Preferential binding of dasatinib to the active form of BCR-ABL unveiled by in silico experiments. Mol Oncol. 2013;7:968-75.

10. Case DA, Darden TA, Cheatham TE III, Simmerling CL, Wang J, Duke RE, et al. AMBER 9, University of California, San Francisco, USA; 2006.

11. Case DA, Darden TA, Cheatham TE III, Simmerling CL, Wang J, Duke RE, et al. AMBER 11, University of California, San Francisco, USA; 2010.

12. a) Chimera (v.1.4), Resource for Biocomputing, Visualization, and Informatics at the University of California, San Francisco (CA), USA.; b) Pettersen EF, Goddard TD, Huang CC, Couch GS, Greenblatt DM, Meng EC, Ferrin TE. J Comput Chem 2004;25:1605-1612.

13. Nagar B, Bornmann WG, Pellicena P, Schindler T, Veach DR, Miller WT, et al. Crystal structures of the kinase domain of c-Abl in complex with the small molecule inhibitors PD173955 and imatinib (STI-571). Cancer Res 2002;62:4236-4243.
14. Tokarski JS, Newitt JA, Chang CY, Cheng JD, Wittekind M, Kiefer SE, et al. The structure of Dasatinib (BMS-354825) bound to activated ABL kinase domain elucidates its inhibitory activity against imatinib-resistant ABL mutants. Cancer Res 2006;66:5790-5797.
15. Modugno M, Casale E, Soncini C, Rosettani P, Colombo R, Lupi R, et al. Crystal structure of the T315I Abl mutant in complex with the aurora kinases inhibitor PHA-739358. Cancer Res 2007;67:7987-7990.
16. Zhou T, Commodore L, Huang WS, Wang Y, Thomas M, Keats J, et al. Structural mechanism of the Pan-BCR-ABL inhibitor ponatinib (AP24534): lessons for overcoming kinase inhibitor resistance. Chem Biol Drug Des 2011;77:1-11.
17. O'Hare T, Shakespeare WC, Zhu X, Eide CA, Rivera VM, Wang F, et al. AP24534, a pan-BCR-ABL inhibitor for chronic myeloid leukemia, potently inhibits the T315I mutant and overcomes mutation-based resistance. Cancer Cell 2009;16:401-412.
18. Duan Y, Wu C, Chowdhury S, Lee MC, Xiong G, Zhang W, Yang R, Cieplak P, Luo R, Lee T. A point-charge force field for molecular mechanics simulations of proteins based on condensed-phase quantum mechanical calculations. J Comput Chem 2003;24:1999-2012.
19. Bayly CI, Cieplak P, Cornell WD, Kollman PA. A well-behaved electrostatic potential based method using charge restraints for determining atom-centered charges: the RESP model. J Phys Chem 1993;97:10269-10280.
20. Singh UC, Kollman PA. An approach to computing electrostatic charges for molecules. J Comput Chem 1984;5:129-145.
21. Besler BH, Merz KM, Kollman PA. Atomic charges derived from semiempirical methods. J Comput Chem 1990;11:431-439.
22. Wang J, Wang W, Kollman PA, Case DA. Automatic atom type and bond type perception in molecular mechanical calculations. J Mol Graph Model 2006;25:247-260.
23. Wang J, Wolf RM, Caldwell JW, Kollman PA, Case DA. Development and testing of a general AMBER force field. J Comput Chem 2004;25:1157-1174.
24. 21. a) Gibbons DL, Pricl S, Kantarjian H, Cortes J, Quintás-Cardama A. The rise and fall of gatekeeper mutations? The BCR-ABL1 T315I paradigm. Cancer 2012;118:293-299; b) Pierotti MA, Tamborini E, Negri T, Pricl S, Pilotti S. Targeted

therapy in GIST: in silico modeling for prediction of resistance. Nat Rev Clin Oncol 2011;8:161-170; c) Dileo P, Pricl S, Tamborini E, Negri T, Stacchiotti S, Gronchi A, et al. Imatinib response in two GIST patients carrying two hitherto functionally uncharacterized PDGFRA mutations: an imaging, biochemical and molecular modeling study. Int J Cancer 2011;128:983-890; d) Pierotti MA, Negri T, Tamborini E, Perrone F, Pricl S, Pilotti S. Targeted therapies: the rare cancer paradigm. Mol Oncol 2010;4:19-37.; e) Conca E, Negri T, Gronchi A, Fumagalli E, Tamborini E, Pavan GM, et al. Activate and resist: L576P-KIT in GIST. Mol Cancer Ther 2009;8:2491-2495; f) Woodman SE, Trent JC, Stemke-Hale K, Lazar AJ, Pricl S, Pavan GM, et al. Activity of dasatinib against L576P KIT mutant melanoma: molecular, cellular, and clinical correlates. Mol Cancer Ther 2009;8:2079-2085; g) Negri T, Pavan GM, Virdis E, Greco A, Fermeglia M, Sandri M, Pricl S, Pierotti MA, Pilotti S, Tamborini E. T670X KIT mutations in gastrointestinal stromal tumors: making sense of missense. J Natl Cancer Inst 2009;101:194-204; h) McAuliffe JC, Wang WL, Pavan GM, Pricl S, Yang D, Chen SS, et al. Unlucky number 13? Differential effects of KIT exon 13 mutation in gastrointestinal stromal tumors. Mol Oncol 2008;2:161-163; k) Tamborini E, Pricl S, Negri T, Lagonigro MS, Miselli F, Greco A, et al. Functional analyses and molecular modeling of two c-Kit mutations responsible for imatinib secondary resistance in GIST patients. Oncogene 2006; 25:6140-6146; i) Pricl S, Fermeglia M, Ferrone M, Tamborini E. T315I-mutated Bcr-Abl in chronic myeloid leukemia and imatinib: insights from a computational study. Mol Cancer Ther 2005;4:1167-1174.

25. Jorgensen WL, Chandrasekhar J, Madura JD, Impey RW, Klein ML. Comparison of simple potential functions for simulating liquid water. J Chem Phys 1983;79:926-935.

26. Berendsen HJC, Postma JPM, Van Gunsteren WF, DiNola A, Haak JR. Molecular-dynamics with coupling to an external bath. J Chem Phys 1984;81:3684-3690.

27. Ryckaert JP, Ciccotti G, Berendsen HJC Numerical integration of the cartesian equations of motion of a system with constraints: molecular dynamics of n-alkanes. J Comput Phys 1977;23:327-341.

28. Toukmaji A, Sagui C, Board J, Darden T. Efficient particle-mesh Ewald based approach to fixed and induced dipolar interactions. J Chem Phys 2000;113:10913-10927.

29. Srinivasan J, Cheatham TE III, Cieplak P, Kollman PA, Case DA. Continuum solvent studies of the stability of DNA, RNA and phosphoramidate-DNA helices. J Am Chem Soc 1998;120:9401-9409.
30. Kollman PA, Massova I, Reyes C, Kuhn B, Huo S, Chong L, et al. Calculating structures and free energies of complex molecules: combining molecular mechanics and continuum models. Acc Chem Res 2000;3:889-897.
31. Gilson MK, Sharp KA, Honig BH. Calculating the electrostatic potential of molecules in solution – method and error assessment. J Comput Chem 1988;9:327-335.
32. Sitkoff D, Sharp KA, Honig BH. Accurate calculation of hydration free energies using macroscopic solvent models. J Phys Chem 1994;98:1978-1988.
33. Sanner MF, Olson AJ, Spehner JC. Reduced surface: an efficient way to compute molecular surfaces. Biopolymers 1996;38:305-320.
34. Andricioaei I, Karplus M. On the calculation of entropy from covariance matrices of the atomic fluctuations. J Chem Phys 2001;115:6289-6292.
35. a) Kroeger Smith MB, Lamb ML, Tirado-Rives J, Jorgensen WL, Michejda CJ, Ruby SK, et al. Monte Carlo calculations on HIV-1 reverse transcriptase complexed with the nonnucleoside inhibitor 8-Cl TIBO: contribution of the L100I and Y181C variants to protein stability and biological activity. Protein Eng 2000;13:413-421; b) Wang J, Morin P, Wang W, Kollman PA. Use of MM-PBSA in reproducing the binding free energies to HIV-1 RT of TIBO derivatives and predicting the binding mode to HIV-1 RT of efavirenz by docking and MM-PBSA. J Am Chem Soc 2001;123:5221-5230.
36. Gohlke H, Kiel C, Case DA. Insights into protein-protein binding by binding free energy calculations and free energy decomposition for the Ras-Raf and Ras-RalGDS complexes. J Mol Biol 2003, 330:891-913.
37. a) Tsui V, Case DA. Theory and applications of the Generalized Born solvation model in macromolecular simulations. Biopolymers 2000, 56:75–291; b) Onufriev A, Bashford D, Case DA. Modification of the generalized born model suitable for macromolecules. J. Phys. Chem. B 2000, 104:3712–3720.

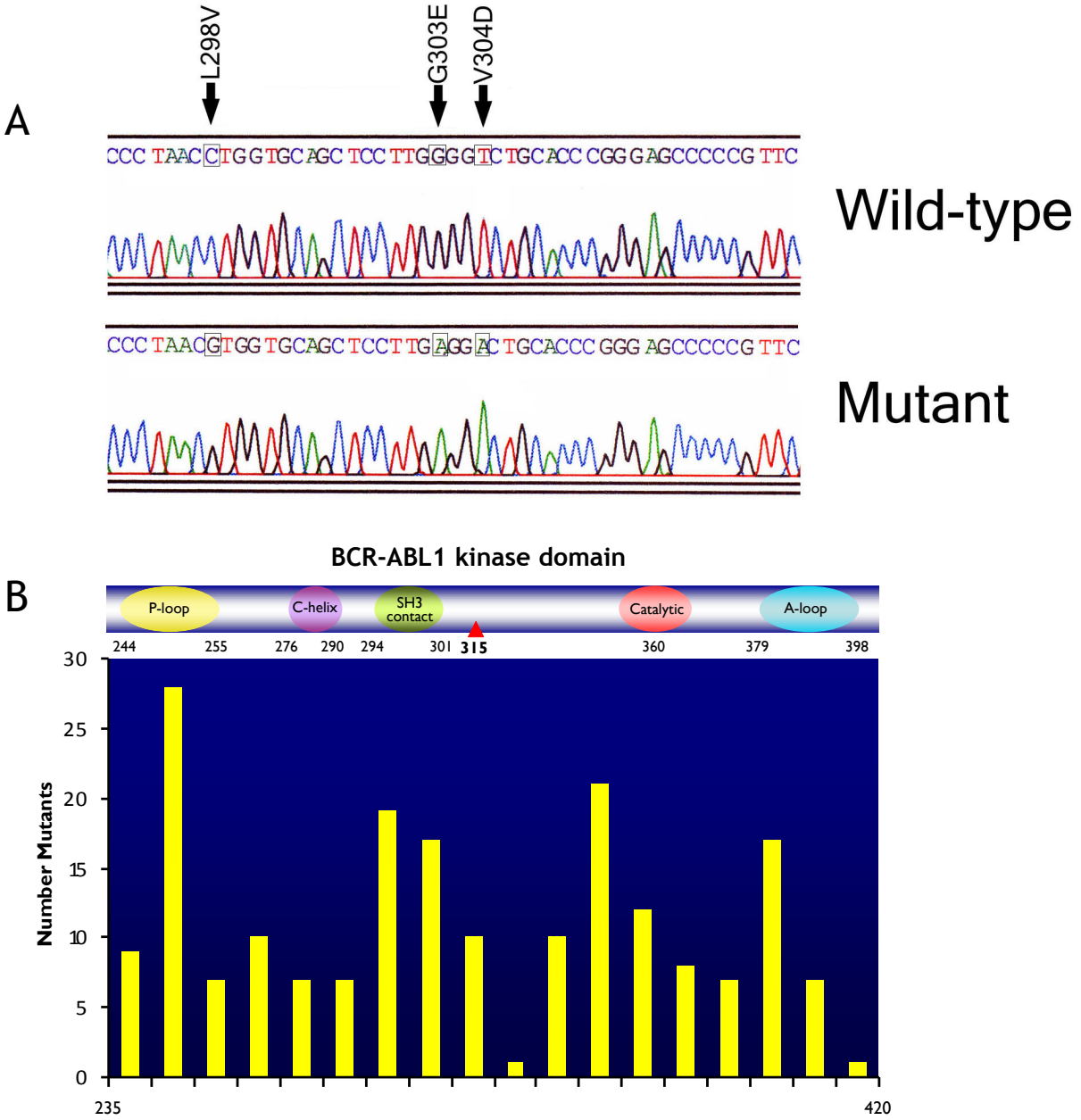

Supplemental Figure 1. ABL1 kinase domain mutations in the study cohort. (A) Chromatogram obtained from a patient after imatinib failure (right before dasatinib therapy was started) carrying 3 different point mutations within the same BCR-ABL1 allele. (B) Topographic representation of the mutations found in patients failing sequential therapy with imatinib followed by dasatinib.

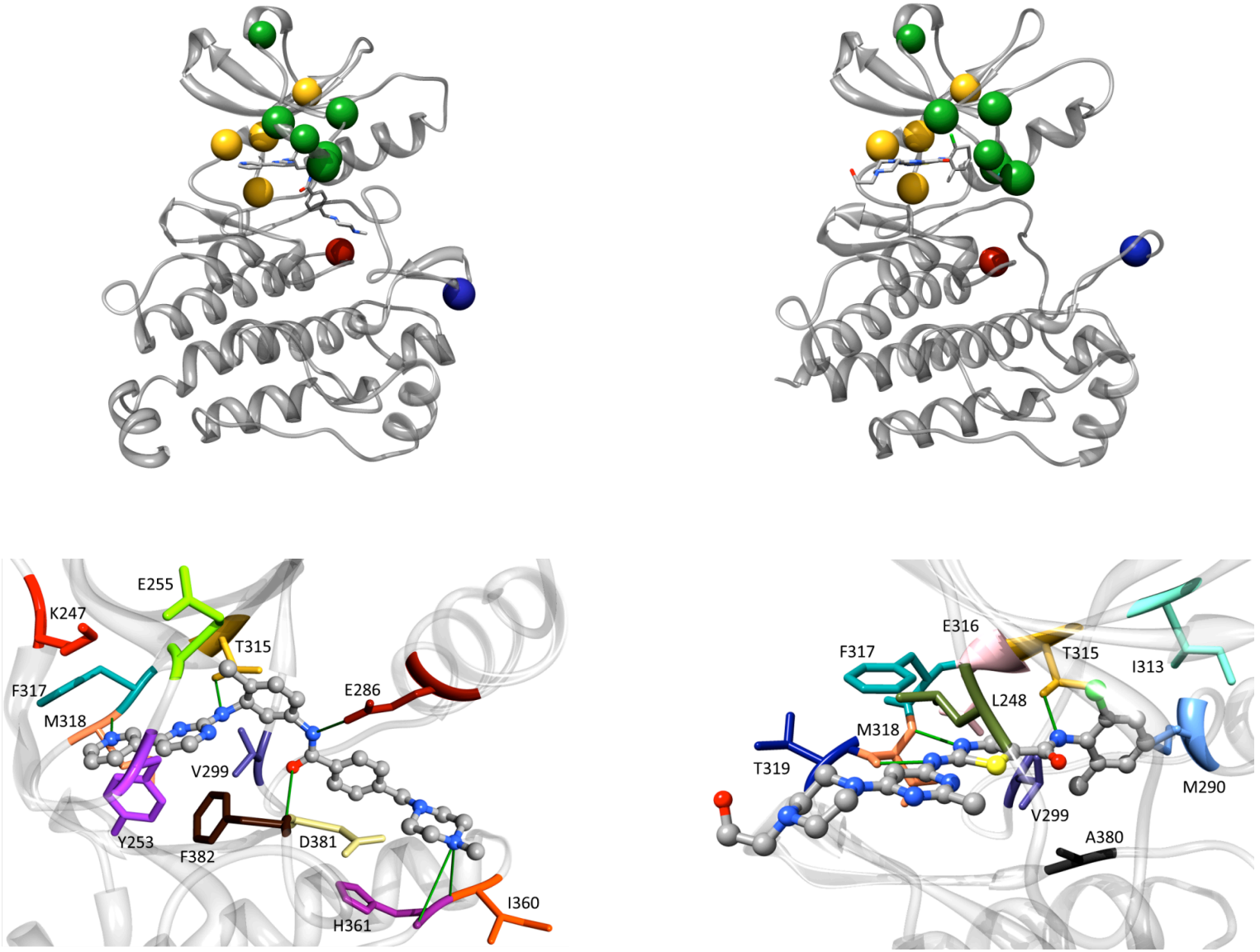

Supplemental Figure 2. Mapping of mutations affecting imatinib and dasatinib binding onto the BCR-ABL1 kinase structure. Top panels: mapping of representative imatinib-resistant mutation sites on the unmutated BCR-ABL1/imatinib complex (left) and unmutated BCR-ABL1/dasatinib complex (right). The secondary structure is highlighted in gray, while the mutant sites are depicted as spheres, with the following color code: forest green (P-loop), gold (hinge region), red, (catalytic loop), and blue (A-loop). Bottom panels: details of the binding site of the unmutated BCR-ABL1 protein in complex with imatinib (left) and dasatinib (right) as obtained from equilibrated MD simulation snapshots. The protein backbone is portrayed as a transparent gray ribbon. The main residues involved in the interaction with each drug are shown as colored sticks and numbered. All hydrogen bonds are shown as green lines. Hydrogen atoms, water molecules, and counterions are omitted for clarity.

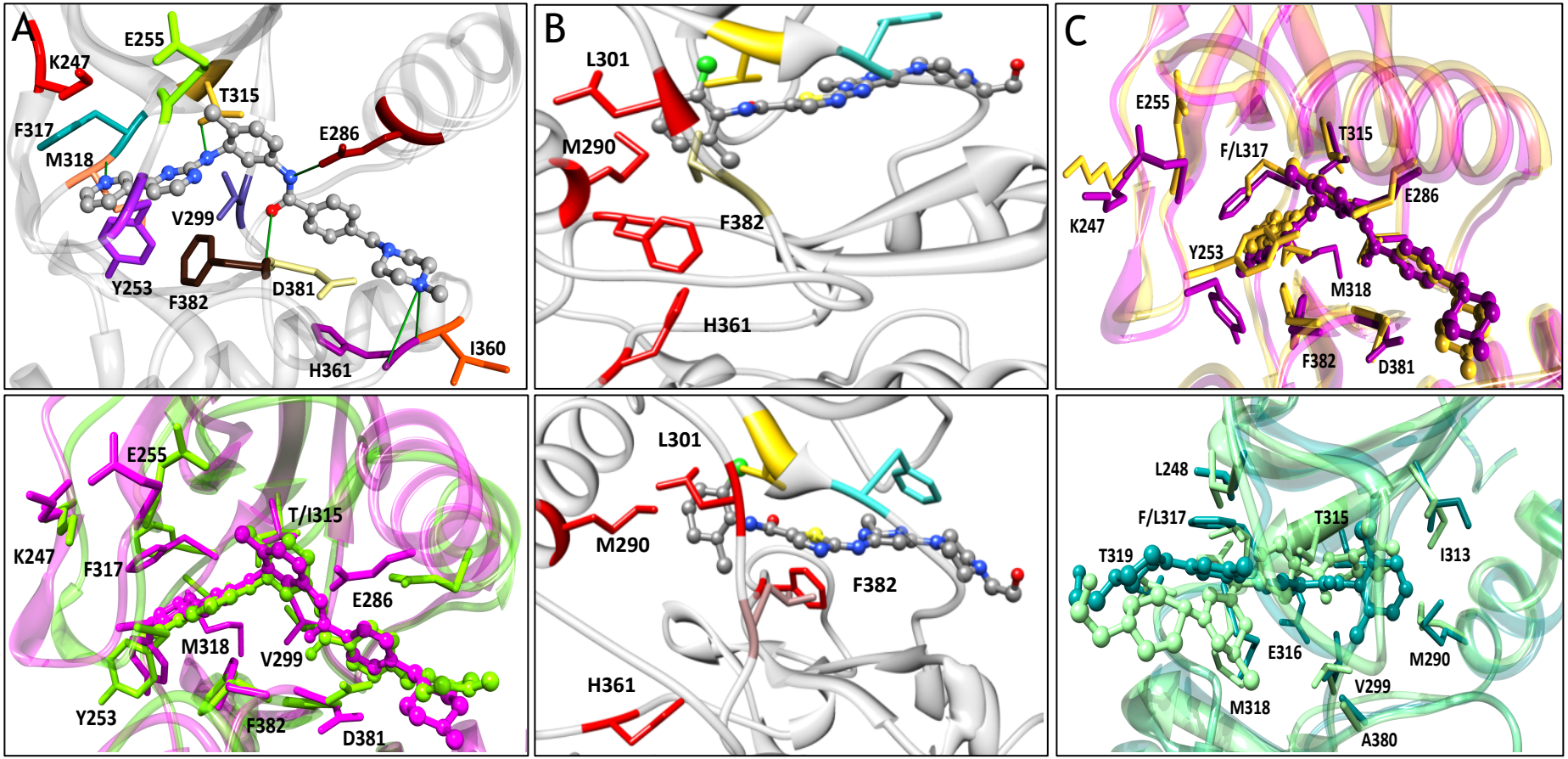

Imatinib		
BCR-ABL1	IC_{50} cal. (nM)	IC_{50} exp. (nM)
Unmutated	21	30[a]
T315I	21000	>5000[a]

Dasatinib		
BCR-ABL1	IC_{50} cal. (nM)	IC_{50} exp. (nM)
Unmutated	0.8	0.6[b]
V299L	960	18[c]

Dasatinib		
BCR-ABL1	IC_{50} cal. (nM)	IC_{50} exp. (nM)
Unmutated	0.8	0.6[b]
F317L	170	18[c]

Supplemental Figure 3. **In silico modeling of ponatinib binding to BCR-ABL1 polymutants. (A)** Top: details of the binding site of unmutated BCR-ABL1 in complex with ponatinib as obtained from equilibrated MD simulation snapshots. The protein backbone is portrayed as a transparent gray ribbon, the main residues involved in drug interactions are shown as labeled colored sticks. Hydrogen bonds are shown as green lines. Middle panel: superposition of the binding site of unmutated BCR-ABL1 (red) and the BCR-ABL1^{T315I} (purple) in complex with ponatinib. In the two complexes, the drug is depicted in red (unmutated) and purple (T315I) sticks-and-balls, respectively. Bottom: superposition of the binding site of unmutated BCR-ABL1 (red) and the BCR-ABL1$^{V299L/F317L}$ double mutant (black) in complex with ponatinib. In the two complexes, the drug is depicted in red (unmutated) and black (F317L/V299L) sticks-and-balls, respectively. **(B)** MD snapshots of dasatinib (top) and ponatinib (bottom) bound BCR-ABL1$^{T315I/F317L}$. The mutant I315 and L317 are depicted as orange and cyan sticks, respectively. Note the marked difference in steric clash (golden areas in both panels), accounting for the higher affinity of ponatinib for the double mutant protein. Hydrogen atoms, water molecules and ions are omitted for clarity. **(C)** Sensitivity of a series of BCR-ABL1 proteins with single point mutations (black bars) or dual mutants (red bars) against ponatinib, based upon calculated IC_{50}. Dotted blue line represents the half maximal inhibitory concentration (IC_{50}) of ponatinib against BCR-ABL1^{T315}.

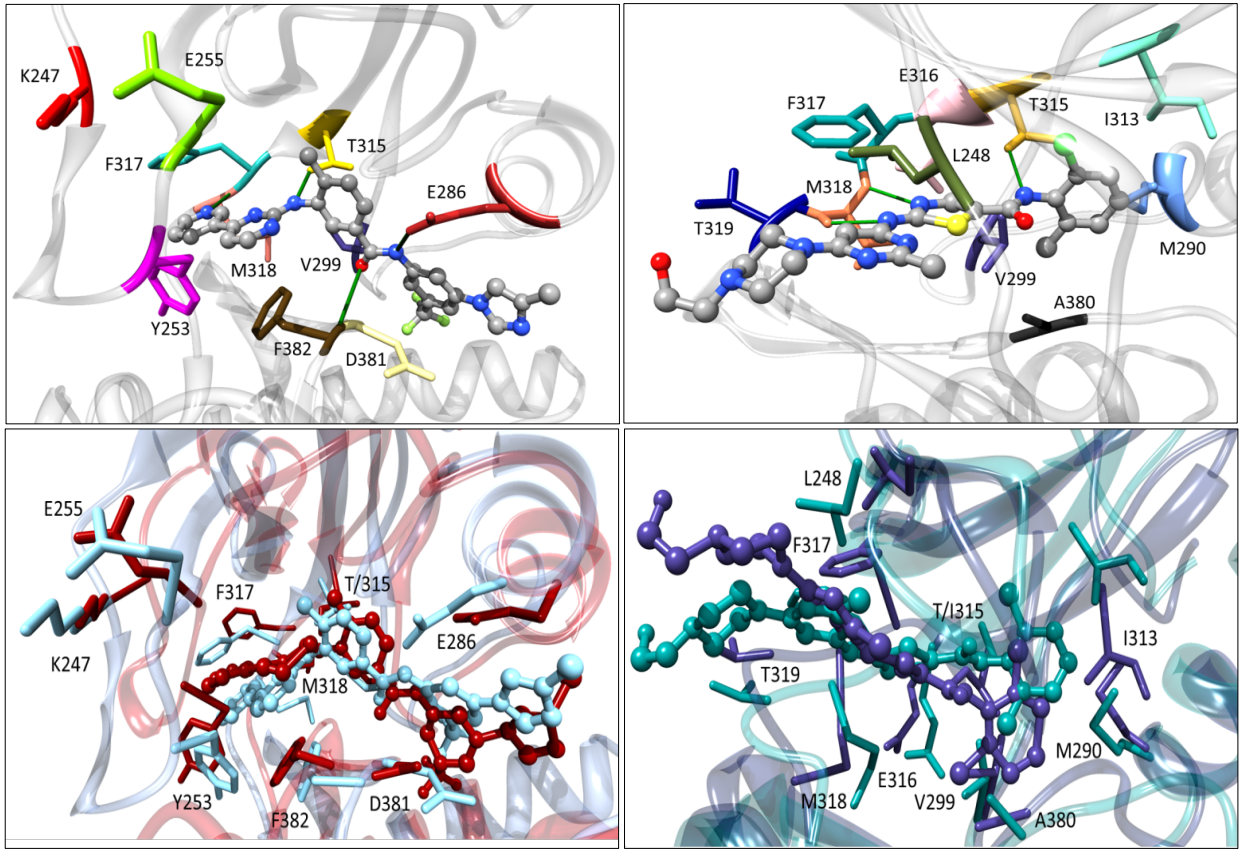

	Nilotinib	
BCR-ABL1	IC_{50} cal. (nM)	IC_{50} exp. (nM)
Unmutated	11	28[a]
T315I	12500	>5000[b]

	Dasatinib	
BCR-ABL1	IC_{50} cal. (nM)	IC_{50} exp. (nM)
Unmutated	0.8	0.6[b]
T315I	19000	>5000[c]

Supplemental Figure 4. Model of nilotinib and dasatinib binding to unmutated or T315I BCR-ABL1. Top panels: details of the binding site of the unmutated BCR-ABL1 kinase domain in complex with nilotinib (left), and dasatinib (right) obtained from equilibrated MD simulation snapshots. The unmutated protein backbone is depicted as a transparent gray ribbon. The main residues involved in the interaction with each drug are shown as colored sticks and labeled. All hydrogen bonds are shown as green lines. Bottom panels: Superposition of the binding site of unmutated BCR-ABL1 (sky blue) and T315I mutant BCR-ABL1 (dark red) in complex with nilotinib (left), and unmutated BCR-ABL1 (dark cyan) and T315I mutant BCR-ABL1 (dark slate blue) in complex with dasatinib (right). In all complexes, the drug is depicted in sky blue and dark cyan (unmutated) and dark red and dark slate blue (T315I) sticks-and-balls, respectively. Hydrogen atoms, water molecules and counterions are omitted for clarity.

[a]Data from Fabbro et al., Biochim Biophys Acta 2010, 1804:454-462. [b]Data from O'Hare el al., PNAS 2008; 105:5507-5512. [c]Data from Puttini et al., Cancer Res 2006; 66:11314-11322.

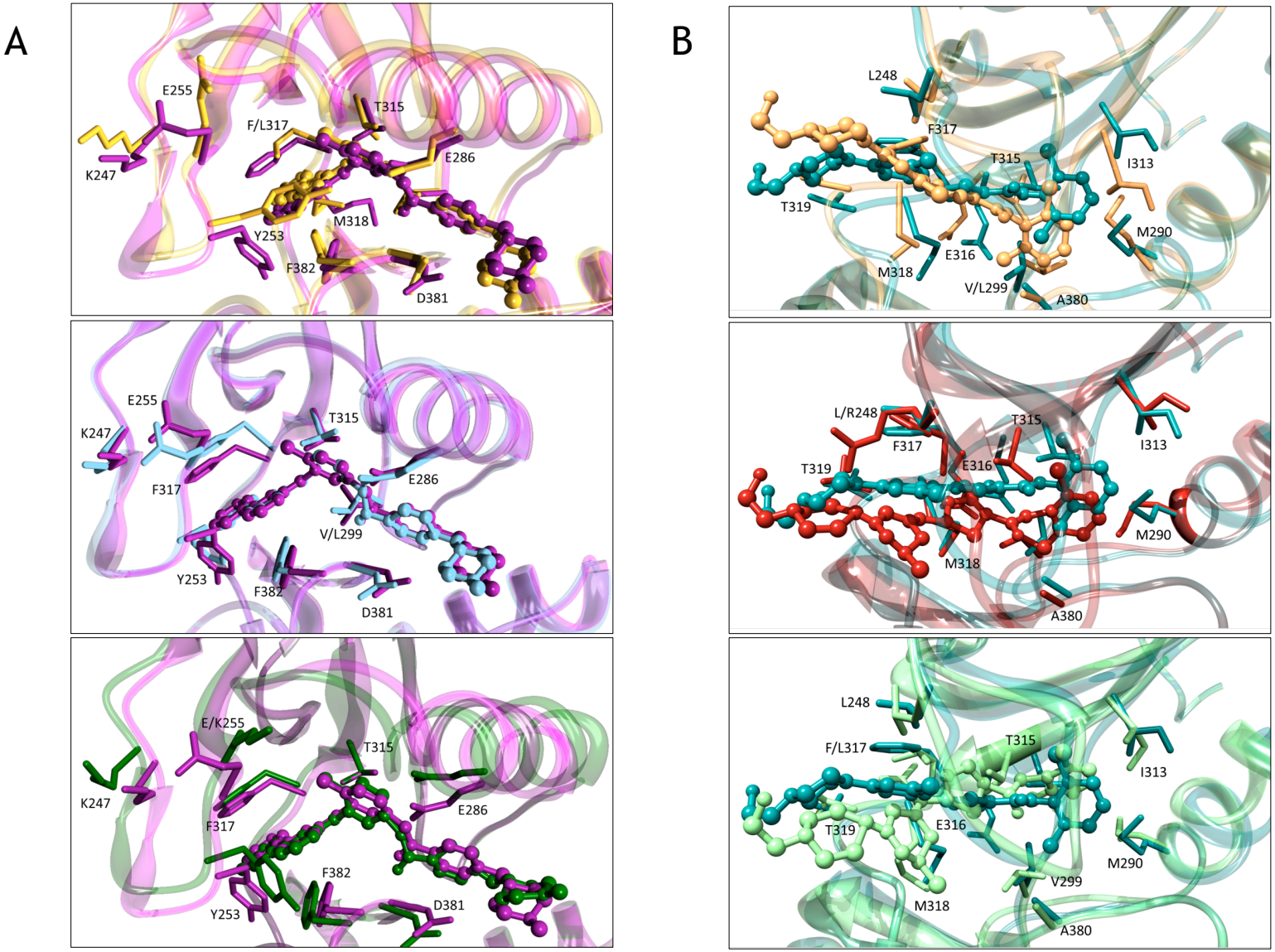

SUPPL FIGURE 5. (A) Top panel: superposition of the binding site of unmutated BCR-ABL1 (dark magenta) and F317L mutant BCR-ABL1 (gold) in complex with imatinib. In the two complexes, the drug is depicted in dark magenta (unmutated) and gold (F317L) sticks-and-balls, respectively. Middle panel: superposition of the binding site of unmutated BCR-ABL1 (dark magenta) and V299L mutant BCR-ABL1 (light blue) in complex with imatinib. In the two complexes, the drug is depicted in dark magenta (WT) and light blue (V299L) sticks-and-balls, respectively. Bottom panel: superposition of the binding site of unmutated BCR-ABL1 (dark magenta) and E255K mutant BCR-ABL1 (forest green) in complex with Imatinib. In the two complexes, the drug is depicted in dark magenta (WT) and forest green (E255K) sticks-and-balls, respectively. **(B)** Top panel: superposition of the binding site of unmutated BCR-ABL1 (dark cyan) and V299L mutant BCR-ABL1 (sand) in complex with dasatinib. In the two complexes, the drug is depicted in dark cyan (unmutated) and sand (V299L) sticks-and-balls, respectively. Middle panel: superposition of the binding site of unmutated BCR-ABL1 (dark cyan) and L248R mutant BCR-ABL1 (firebrick) in complex with dasatinib. In the two complexes, the drug is depicted in dark cyan (unmutated) and firebrick (L248R) sticks-and-balls, respectively. Bottom panel: superposition of the binding site of unmutated BCR-ABL1 (dark cyan) and F317L mutant BCR-ABL1 (light green) in complex with dasatinib. In the two complexes, the drug is depicted in dark cyan (unmutated) and light green (F317) sticks-and-balls, respectively. Hydrogen atoms, water molecules and counterions are omitted for clarity in all panels.

[a]Data from Corbin et al., Blood 2003, 101:4611-4614.

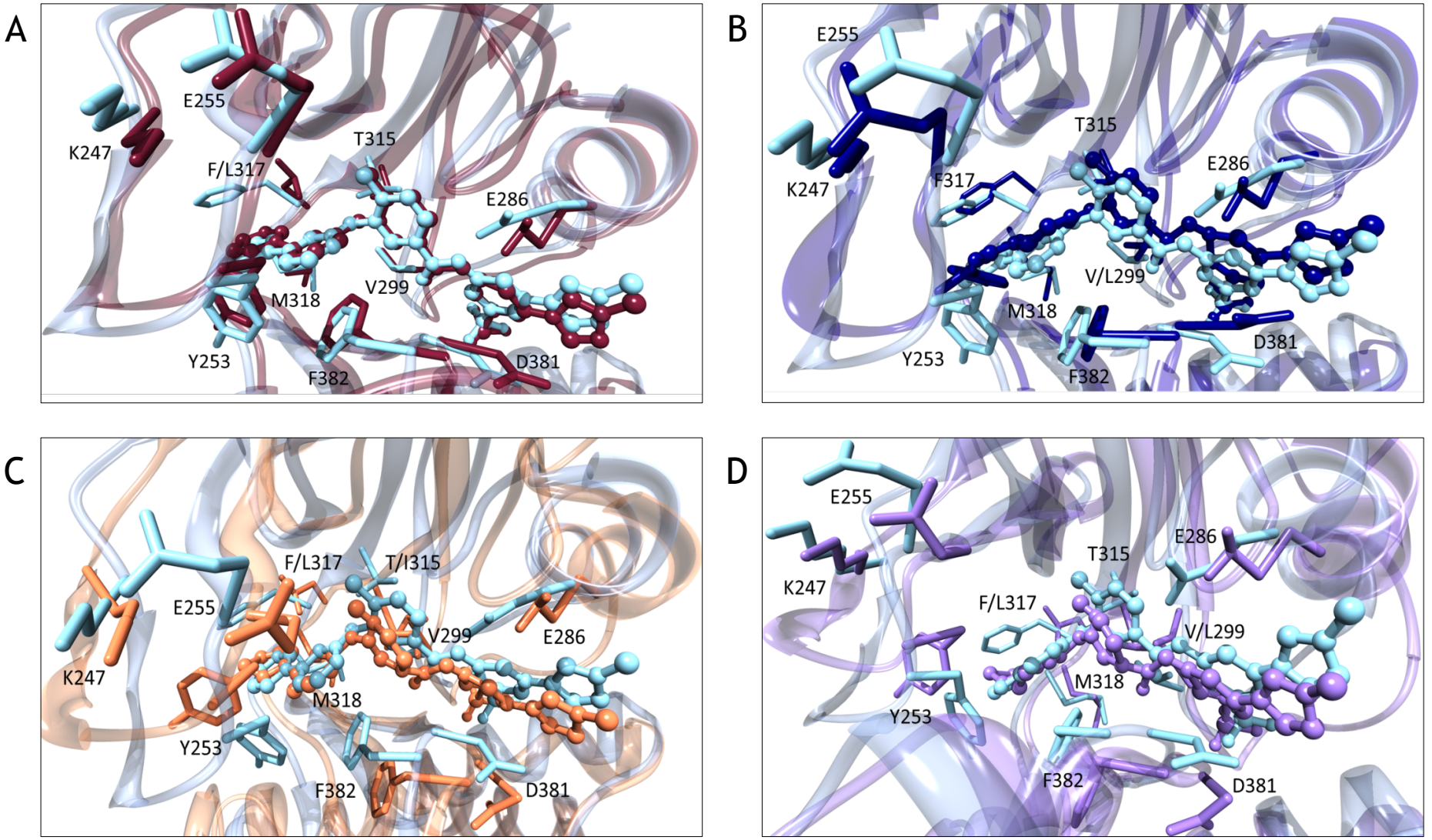

Supplemental Figure 6. Model of nilotinib binding to unmutated, F317L, V299L, F317L/T315I, and F317L/V299L BCR-ABL1.(A) Superposition of the binding site of unmutated BCR-ABL1 (sky blue) and F317L mutant BCR-ABL1 (dark plum) in complex with nilotinib. In the two complexes, the drug is depicted in sky blue (unmutated) and dark plum (F317L) sticks-and-balls, respectively. (B) Superposition of the binding site of unmutated BCR-ABL1 (sky blue) and V299L mutant BCR-ABL1 (dark blue) in complex with nilotinib. In the two complexes, the drug is depicted in sky blue (unmutated) or dark blue (V299L) sticks-and-balls, respectively. (C) Superposition of the binding site of unmutated BCR-ABL1 (sky blue) and the F317L/T315I double mutant BCR-ABL1 (coral) in complex with nilotinib. In the two complexes, the drug is depicted in sky blue (unmutated) and coral (F317L/T315I) sticks-and-balls, respectively. (D) Superposition of the binding site of unmutated BCR-ABL1 (sky blue) and F317/V299L mutant BCR-ABL1 (medium purple) in complex with nilotinib. In the two complexes, the drug is depicted in sky blue (unmutated) and medium purple (F317L/V299L) sticks-and-balls, respectively. Hydrogen atoms, water molecules and counterions are omitted for clarity in all panels.

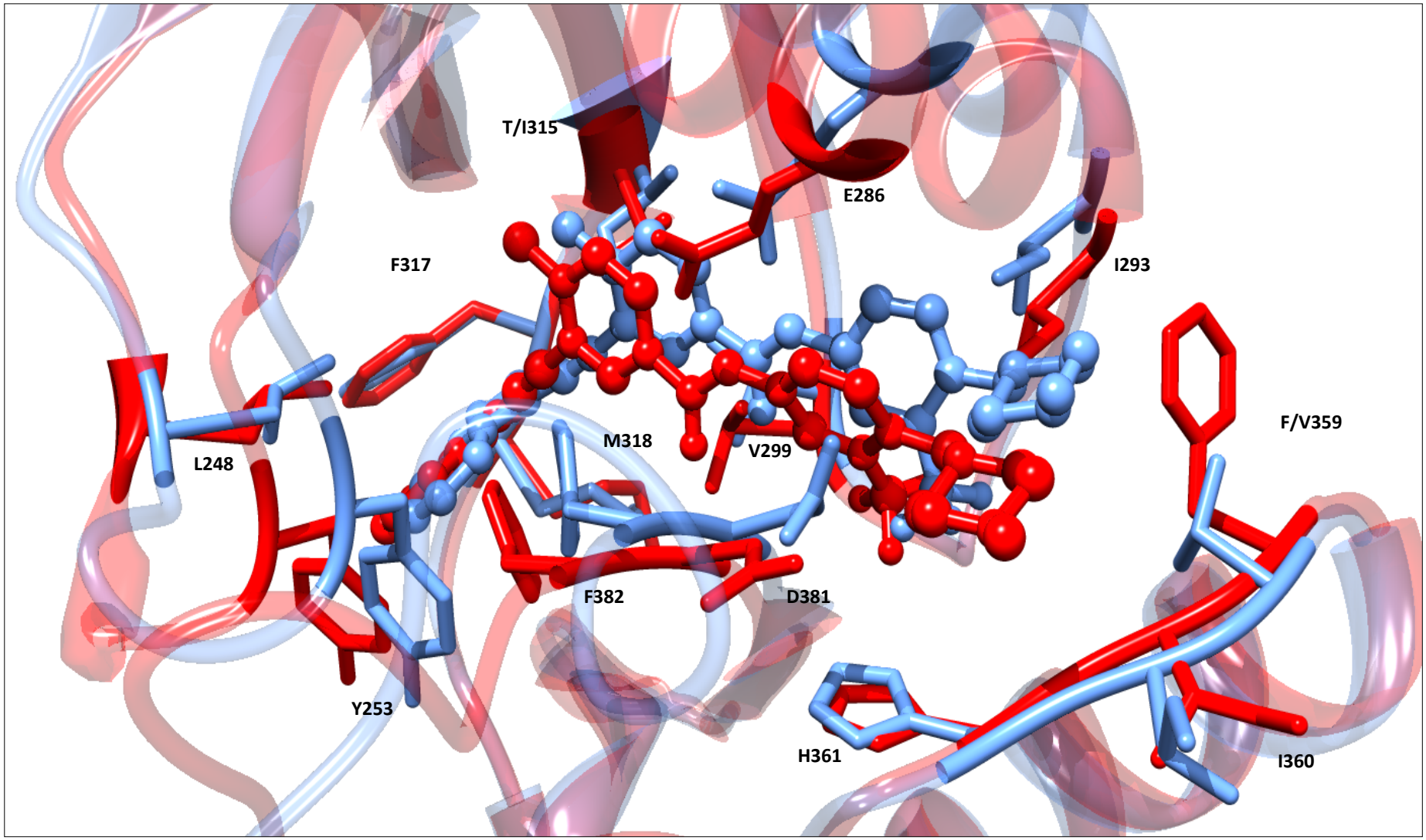

Figure 7. Superposition of the binding site of unmutated BCR-ABL1 (red) and the T315I/F359V double mutant BCR-ABL1 (cornflower blue) in complex with ponatinib. The drug is depicted in red (unmutated) and cornflower blue (T315I/F359V) sticks-and-balls, respectively. All main residues involved in ponatinib binding are labeled.

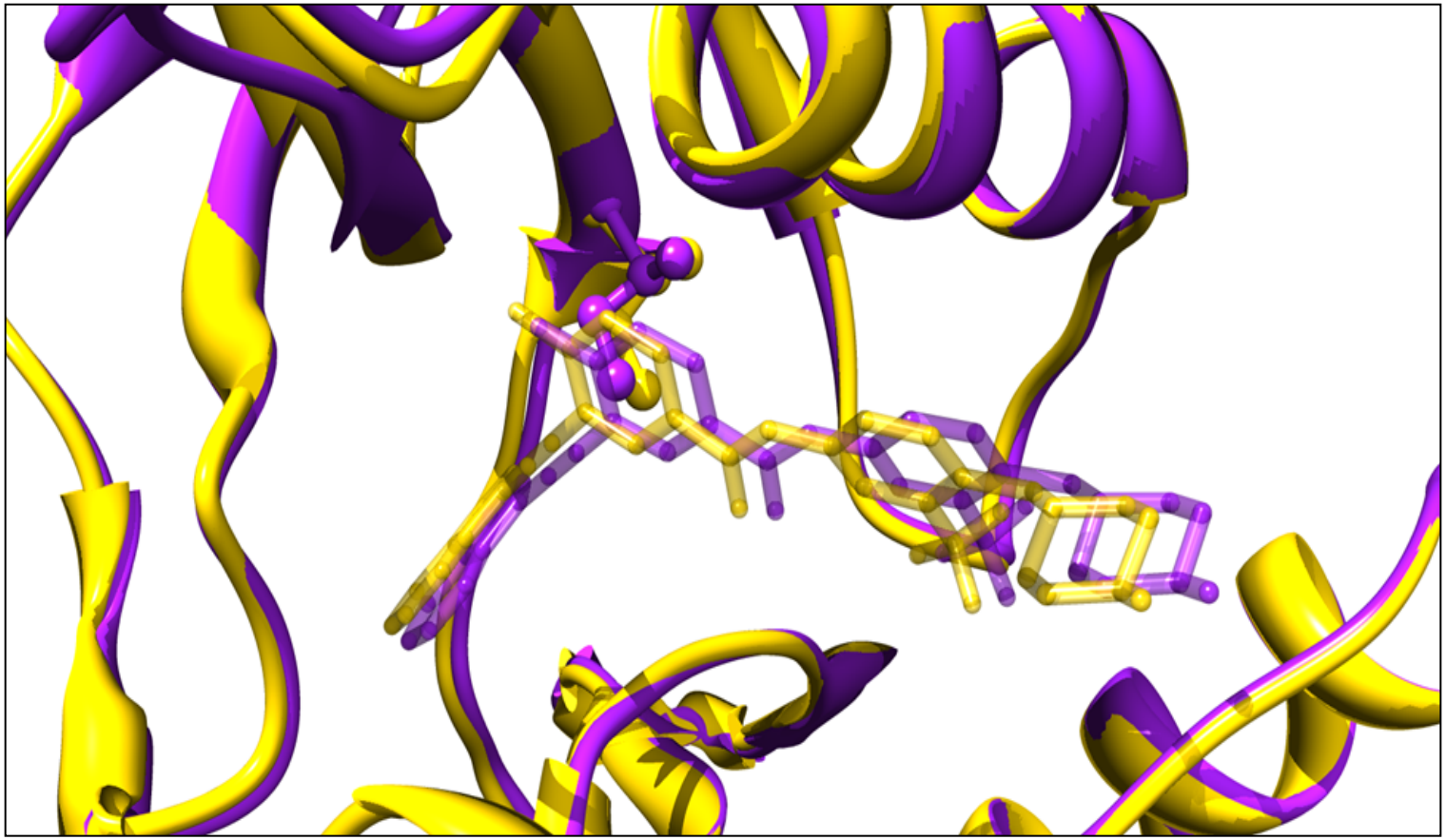

Supplemental Figure 8. Comparison between an equilibrated molecular dynamics (MD) snapshot of the T315I mutant BCR-ABL1 in complex with ponatinib as obtained using the available crystal structure 3IK3.pdb (purple) and from our computational mutagenesis procedure[15] (gold). The kinase is in a ribbon representation , whereas ponatinib is shown in correspondingly colored sticks. Water, ions and counterions are omitted for clarity. For details of the MD conditions, see Supplementary results appendix.

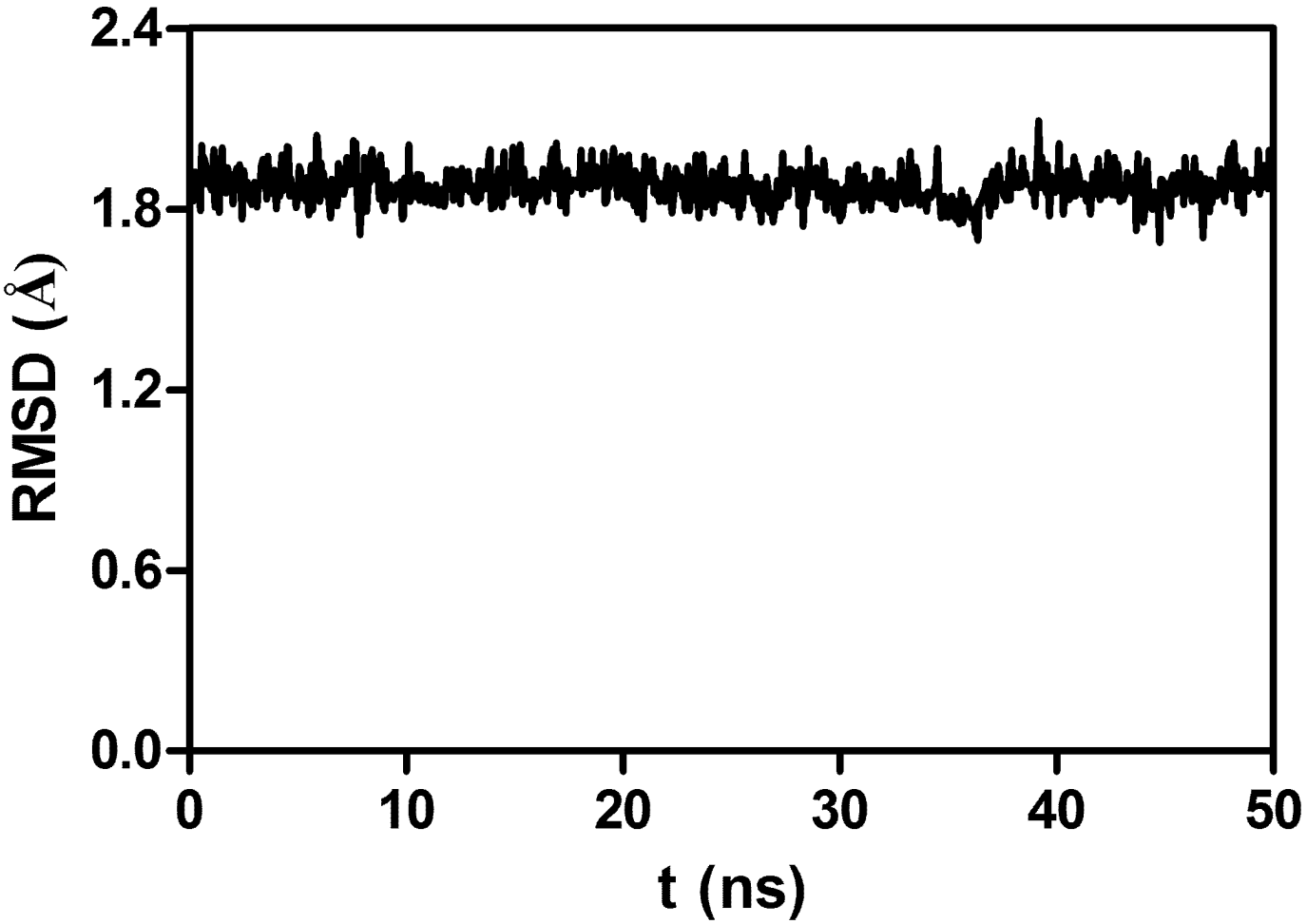

Supplemental Figure 9. Stability of the BCR-ABL1/inhibitor complex during the MD trajectories. (A) Root-mean-square deviation of the coordinates of the backbone atoms of the wild type BCR-ABL1 kinase in complex with imatinib along the 50 ns MD simulation compared with those of the initial structure.